ANATOMIA HISTOLOGIA EMBRYOLOGIA
JOURNAL OF VETERINARY MEDICINE

Anat. Histol. Embryol. **37**, 205–213 (2008)
ISSN 0340–2096

doi: 10.1111/j.1439-0264.2007.00830.x

Institute of Veterinary Pathology, Chair of General Pathology and Neuropathology, Ludwig-Maximilians University, Munich, Germany

Stereological Characteristics of the Equine Accessory Nerve

K. Matiasek[1]*, P. Gais[2], K. Rodenacker[3], U. Jütting[3], J. J. Tanck[4] and W. Schmahl[4]

Addresses of authors: [1]Neuropathology Laboratory, Diagnostic Laboratory Services, The Animal Health Trust, Lanwades Park, Kentfort, Suffolk CB8 7UU, UK; [2]Institute of Pathology, GSF National Research Centre for Environment and Health, Ingolstädter Landstr. 1, 85764 Neuherberg, Germany; [3]Institute of Biomathematics and Biometry, GSF National Research Centre for Environment and Health, Ingolstädter Landstr. 1, 85764 Neuherberg, Germany; [4]Institute of Veterinary Pathology, Chair of General Pathology and Neuropathology, Ludwig-Maximilians University, Veterinar Str. 13, 80539 Munich, Germany; *Corresponding author: Tel.: +44 1638 751000; fax: +44 1638 750410; e-mail: kaspar.matiasek@neuropath.org.uk

With 9 figures and 2 tables

Received October 2007; accepted for publication November 2007

Summary

Stereological techniques have been increasingly employed for assessment and characterization of neuromuscular diseases in humans and animals. As an adjunct to histopathology, morphometrical algorithms provide quantitative evidence of the peripheral nerve composition, thereby shedding light on its fibre characteristics and basic electrophysiological properties. In the horse, stereological investigations already have focussed on the recurrent laryngeal, deep peroneal and lateral palmar nerves (LPN). Of these, only the latter is suitable for taking biopsies in clinical settings, however, it does not contain any motor fibres and Ia-afferents. On account of its virtually mixed fibre qualities, most researchers today recommend the cervical branch of the equine accessory nerve (AN) for harvesting diagnostic samples. Thus, the present study was carried out to gain morphometrical proof of the AN composition and to obtain stereological base values in healthy individuals using state-of-the-art technology. All parameters were compared to the common peroneal nerve (CPN), known to harbour all myelinated fibre classes. As this second biopsy site is located farther distally to the neuro-axis, attention was paid to possible length-dependent features.

Taken together, digital image analysis could be accurately applied on all AN samples. Stereology supported the histological and clinical evidence that the AN contains all myelinated fibre types. The huge range and scatter of fibre counts and density (3351–17 812/mm^2) per fascicle were comparable to that measured in the equine common peroneal, deep peroneal, lateral palmar and recurrent laryngeal nerves. Similar to those, fibre diameter distribution was bimodal with slow Aβ- and Aγ-mechanoceptor afferents outnumbering large myelinated Aα-fibres by a factor of about 1.5. With a *g-ratio* at 0.55 ± 0.001, the overall degree of myelination in the AN is highly consistent and insignificantly ranges between that of the equine common peroneal and LPNs. Apart from this subtle deviation, a statistically relevant difference between the more proximal AN and the distal CPN could not be documented. By obtaining morphometrical standard parameters and even more sophisticated distribution indices, stereology is a valuable tool for detection of subtle changes that are likely to escape from the investigators' eyes. The AN serves as a reliable source for advanced peripheral nerve research and should be accompanied by farther distal nerve probes for assessment of neuropathies that present with a proximodistal gradient.

Introduction

During the late 90s much effort had been launched to establish computed algorithms as a diagnostic aid for quantification of peripheral nerve system components (Geuna et al., 1999). Out of the plethora of different morphometrical approaches, assessment of nerve fibre number, density and size, as well as the myelin sheath thickness became part of advanced neurodiagnostics. Those parameters reflect the electrophysiological properties of a peripheral nerve that are linked to the number, amount and relation of its conductive and insulating components (Vleggeert-Lankamp et al., 2004). Thus, peripheral nerve morphometry provides an insight not only in pathological shift of nerve fibre composition but also into electro-functional consequences that have an impact on nerve conduction velocity, amplitude of compound action potentials, firing threshold (Fields and Ellisman, 1986) and refractory period (Smith, 1978). Morphometrical techniques have already been introduced into experimental nerve research (Vleggeert-Lankamp et al., 2004) and into phenotyping of genetically engineered laboratory animals. Their application in nerve biopsies in clinical settings still hampers from the difficulty to avoid artefacts that preclude full-automatic assessment (Urso-Baiarda and Grobbelaar, 2006). Even with sparse deformation image analysis remains time-consuming, the method requires numerous interactive steps exceeding the time frames and manpower of a routine diagnostic service. If the investigator were to overcome those limitations, this person still has to face the paucity of control values for individual nerves matched for species, strain or breed, gender and age (Dyck et al., 1984). Thus, a neuromorphometrical database is desirable, especially for those species where neurological disabilities are not easily assessable through clinical testing (Wheeler, 1987).

Morphometrical studies had been carried out on a variety of peripheral nerves in the horse (Cahill et al., 1986; Duncan et al., 1974; Slocombe et al., 1992). However, Wheeler was the first to perform electrophysiological and morphometrical analysis on an equine peripheral nerve that is suitable for biopsy and does not bear the risk of limb dysfunction (Wheeler, 1987). Focussing on the LPN, he documented a

fibre content comparable to that of human sural nerves. Although the LPN meets all requirements for morphometrical analysis, it completely lacks motor axons and Ia/b-fibres. This restriction renders its representativity for large fibre conditions questionable. When it was recognized that the cervical component of the equine accessory nerve (AN) is profoundly affected in equine motor neuron disease (EMND) another, more promising biopsy site was established (Cummings et al., 1990). In advanced stages of EMND, this branch shows a positive predictive value of 77.4%, while with a histologically inconspicuous biopsy the probability that a horse does not have EMND is 90% (Jackson et al., 1996).

The remaining false-negative evaluations might depend on the stage of disease or the inability even of experienced researchers to detect subtle changes amidst histological parameters that underlie significant intra- and inter-individual variations, or even artefact (Pamphlett and Sjarif, 2003). Given that the respective nerve segments had been characterized in healthy subjects, digital image analysis may provide a clue to deciphering shifts in nerve fibre configuration and content and, thereby, help to detect and characterize 'sub- and pre-morphological' neuropathies.

In turn, this study was carried out to gain morphometrical proof of the fibre composition of the healthy equine AN. As this nerve, on clinical and histological base, seems to harbour all myelinated fibre classes, the values were directly compared to the common peroneal nerve (CPN) which, throughout species, is the prototype of a mixed nerve and virtually mirrors all systemic neuropathies; even those that are restricted to one single fibre type.

Further, the CPN is rather protected from incidental trauma, easily accessible at a standardized location and can be evaluated from a reasonable number of fascicles harvested by fascicular sampling. Therefore, the peroneal nerve already had been considered a representative source of information in studies on Australian stringhalt (Slocombe et al., 1992) and laryngeal hemiplegia (Cahill et al., 1986; Duncan, 1992).

Given their different distances to the central nervous system, comparison between the accessory and peroneal biopsy sites is likely to uncover length-dependent features, as well. The diagnostic yield of relevant morphometrical parameters is outlined in the text, whereas age-related variations are featured in another study.

Material and Methods

Animals, sampling and tissue processing

This study was carried out on nerve samples collected from 8 German standard-bred horses (2.5 months to 18 years; mean 9.7) in which neurological disorders had been excluded through clinical examination. Whole trunk specimens of the peroneal nerve and the ventral branch of the spinal AN were excised immediately after euthanasia. A detailed approach has been described elsewhere (Jackson et al., 1996).

In short, sternocephalicus muscle was retracted to expose its dorsomedial surface where the ventral branch of the AN enters the muscle near the musculotendinous junction. Then, sternocephalicus muscle was incised longitudinally, allowing the excision of a 3- to 5-cm nerve segment.

The CPN was exposed by lateral transection and retraction of the caudal and lateral insertions of biceps femoris muscle. After identifying the distal peroneal bifurcation, a piece of 3- to 5-cm length was harvested from proximally adjacent segments of the common nerve trunk.

Once obtained, each nerve sample was examined macroscopically and gently freed from surrounding fat and fibrous epineurium after dipping into collagenolytic glycine buffer (Adams et al., 1968). Single fascicles were identified under a dissection microscope, and separated tension-free after transection of mesoneurial adhesions. Several of these fascicles were stretched on a sheet of paper and immersed in 2.5% glutaraldehyde in 0.1 M Sorensen's phosphate buffer (pH 7.4) for 1–2 h at room temperature. After fixation, samples were rinsed with Sorensen's buffer, cut transversally with a razor blade into five segments of 3-mm length and incubated again in Sorensen's buffer for 24 h at 4°C. Thereby, some longitudinal variations could be assessed over a 1.5-cm distance per fascicle. Nerve segments underwent post-fixation in 2% OsO_4 for 2 h at room temperature, repeated buffer rinses and a graded alcohol series before being embedded in epoxy resin. For routine histological inspection, semi thin sections (0.5 μm) were mounted on triethoxysilane-coated glass slides and stained with azur II-methylene blue-safranin (AS).

Only cross sections of entire fascicles meeting the criteria of a summarized endoneurial area larger than 100 000 μm^2 and a maximal mechanical distortion, defined as artificial crush injury, of 6% endoneurial tissue were included in the evaluation (Sundkvist et al., 2000).

Stereological techniques were applied on semi-thin slices (Da Silva et al., 2006) adjacent to suitable AS-specimens, after staining with myelin-specific *p*-phenylene diamine (PPD) (Schultze, 1972).

Image analysis

Image acquisition

Photomicrographs of at least four fascicles per nerve sample were taken by a Zeiss Axiovert 100® light microscope equipped with a PLANAPO oil immersion objective (100×, n.A. 1.25), a CCD camera (512 × 512 pixels) and a motorized stage. In order to provide a whole cross section of the fascicle, individual images were assembled automatically (LMS410-software, Mannweiler, GSF) and scaled into mosaic pictures of 1024 × 1024 pixels. According to the number of tessels, pixel sizes ranged between 0.0404 μm^2 (3 × 3) and 0.3636 μm^2 (9 × 9), while the inter-pixel distance corresponded to 0.201-μm minimum and 0.603-μm maximum.

Image processing

Interactive processing was performed by LEICA- and QWIN software Routine NERSM.Q5R (Gais, GSF). Image processing included the following steps: (1) adjustment of threshold levels; (2) transformation into a simplified binary image; (3) separation of adjacent fibres; (4) elimination of false fibres; (5) application of the morphometrical operator (Fig. 1).

Adjustment of threshold levels. During image analysis, each pixel has to be classified into black (myelin) and white (non-myelin). Even after myelin-specific PPD staining inhomogeneous background remains a possible source of false detection and has to be cleared (Romero et al., 2000). Differences between grey levels of axoplasm and endoneurial matrix were

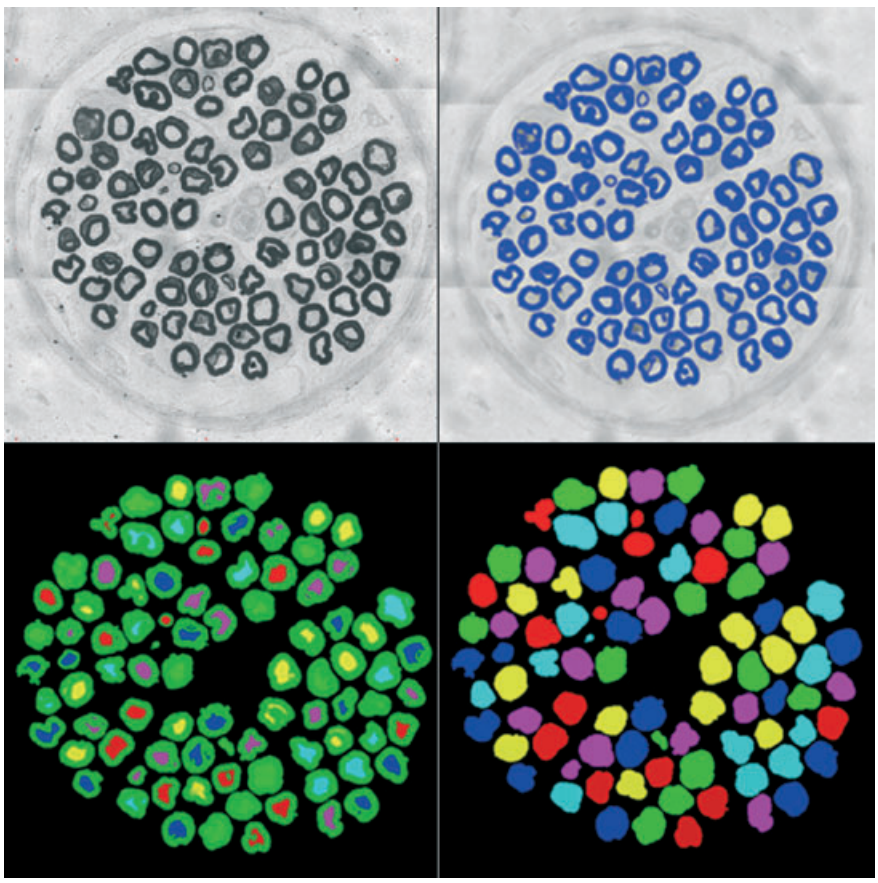

Fig. 1. Stepwise segmentation of tessellated photomicrographs. After detection of black stained myelin sheath (upper pictures), the background was merged and subtracted. Areas larger than 2 μm diameter, completely encircled by myelin sheath, were considered as axonal compartment (lower, left). All pixels encompassed by the outer myelin border were counted for assessment of total fibre size (lower right).

merged until histograms appeared with two peaks only, comprising myelin and non-myelin substance. Thereby, a simplified binary image was generated (Fig. 1) (Da Silva et al., 2006).

Interactive image correction. Incomplete fibres were joined up, touching fibres were separated, and any debris mimicking myelinated fibres was deleted with an interactive eraser tool. In addition, severely distorted fibres as well as nodal and paranodal cross sections were excluded from being measured. As adjacent nerve fibres with touching myelin sheaths were seldom encountered Euclidian distance transformation proposed for tightly packed fascicles (Romero et al., 2000) could be avoided. Black spots of non-myelin origin as well as distorted nerve fibres were removed from the binary picture. Images were considered adequate for further processing if more than 97% of peripheral nerve fibres were suitable for image analysis.

Application of the morphometrical operator. Persistent artefacts were reduced by connected operators' filtering. Thereby, objects were screened separately and together with their neighbours. A nerve fibre was defined by (1) a bright centre surrounded by a black ring, plus (2) a diameter of at least 2 μm. In contrast to other studies (Romero et al., 2000), Schmidt-Lanterman incisures did not interfere with assessment of the myelin sheath diameter (Tanck, 2004).

Analysis

Quantification of nerve fascicle composition included (1) direct measurement of histological structures, and (2) calculation of indirect values. Amongst morphometrical parameters reference area, nerve fibre counts, areas and perimeters of whole fibres/axons/myelin sheaths, myelin sheath thickness and fibre distances were read from modified binary images by application of the software MT_O_P program (IDL (Research System Inc., Boulder, CO, USA) (Rodenacker and Bengtsson, 2003). Another set, of indirect parameters, comprising nerve fibre density, axon and whole fibre diameters, and circularity, *g-ratio* as well as the percentage of large and small myelinated fibres were calculated from previously obtained values.

For determination of *nerve fibre density* all measurable fibres (resembling axon plus myelin profiles) of one fascicle were included. In order to overcome perineurial disruption and artificial widening of sub-perineurial spaces, *reference area* was not defined as the area circumscribed by perineurial layer but by a line drawn around peripheral aspects of outermost nerve fibres (Fig. 2). This boundary was set automatically by a digital mask.

Amongst single fibre parameters fibre *size* was determined by counting the pixels occupying the cross sectional profile of each fibre (Fig. 3), and by calculating the fibre *diameter*. The latter proved to be most reliable (Tanck, 2004) if obtained from a reconstructed circle with a number of pixels corresponding to the irregularly shaped fibre image (Karnes et al., 1977). Accordingly, the formula for calculating the fibre diameter was: $2\sqrt{(\text{fibre area}/\pi)}$.

Axonal area and *diameter* ($2\sqrt{(\text{axon area}/\pi)}$ were determined in a similar fashion as the whole fibre values. In order to avoid false detection through myelin sheath splitting or clefts, bright foci had to be surrounded completely by black pixels, and to

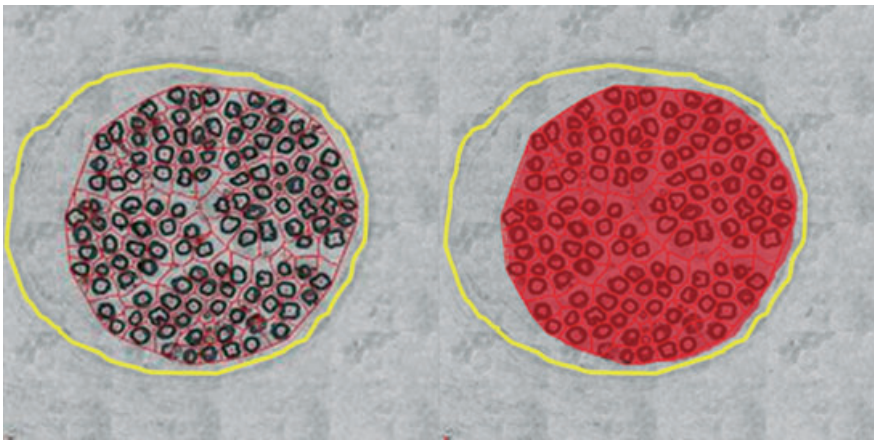

Fig. 2. Only the true endoneurial area (red mask) was chosen as reference area for calculation of nerve fibre density. (Yellow line: perineurial internal surface; greyish area in between yellow line and endoneurium: artificially widened subperineurial space).

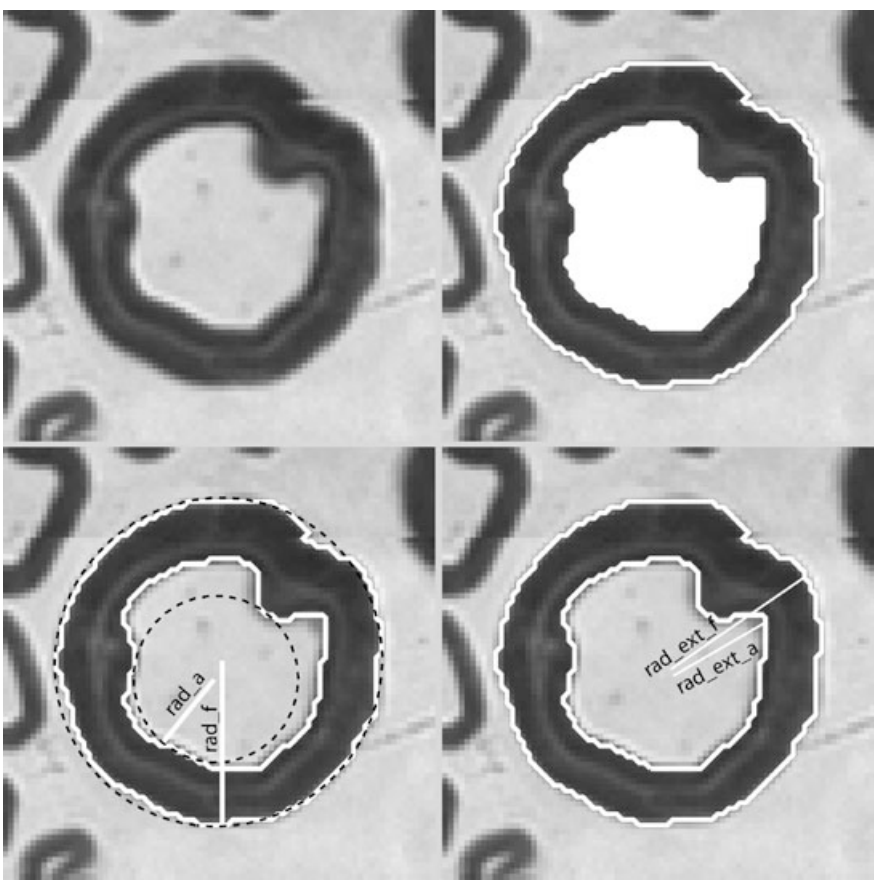

Fig. 3. Fibre and axon sizes both were obtained from pixels counts. Due to deviations from circular shape, the compartment surrounded by inner myelin border much closer reflects true axonal area than square micrometers of the largest inscribed circle (lower, left). Similarly, pixels surrounded by the outer myelin surface (white line) resemble whole fibre area.

reveal a diameter larger than 2 μm to be considered as axons (Romero et al., 2000). Smaller spots were merged.

The degree of myelination per fibre or fascicle was assessed in terms of *g-ratio*, defined as the ratio *axon diameter/fibre diameter*, and the absolute and relative *myelin sheath thickness*. The latter value was obtained from the mean radius of inserted circles into each myelin sheath. A comprehensive description of different morphometrical approaches to myelin sheath parameters is provided elsewhere (Tanck, 2004).

Histograms of myelinated nerve fibres (area or diameter of equivalent area), axons (area or diameter), and myelin sheath (area or thickness) per fascicle and per square millimetre were plotted.

After correction of obliquity, deviation from fibre circularity was investigated by comparison of perimeters of the fibre profile and a circle of equivalent pixel counts $[P^2/(4\pi \times A)]$ (Fig. 4). A true circle exhibits a form factor of 1. Loss of fibre circularity is indicated by values >1. The form factor was obtained from both outer ($P2A^o$) and inner ($P2A^i$) myelin margins.

Statistical analysis

Median and mean of all parameters were calculated and shown with SD. For ratios mean and SD were calculated according to stereological methods (Cochran, 1977). ANOVA was used to

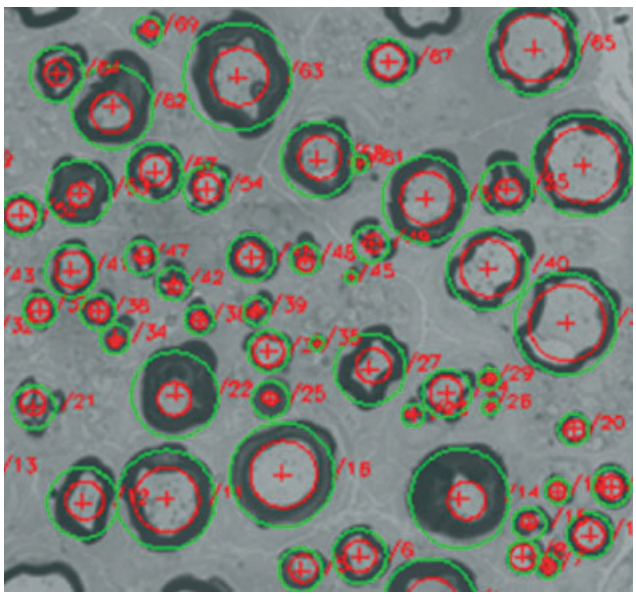

Fig. 4. Fibre and axon diameters were calculated from circles reconstructed from pixel counts.

compare single parameters amongst the different nerve segments, fascicles, nerves, and animals (Bailey, 1981). Paired *t*-test was applied to compare the accessory and CPN values in individuals. The relationship between two parameters was evaluated by Pearson's correlation. Thereby, a *P*-value of 0.05 or less was accepted as indicating significance.

Results

Suitability of histological specimens

In all obtained nerve samples, multiple fascicular cross sections fulfilled the inclusion criteria mentioned above. A minimum of six fascicles per nerve and animal was morphometrically evaluated. The PPD-staining appeared myelin-specific with minor background staining in a few slices and did, therefore, not preclude semi-automatic assessment. Interactive image segmentation was performed within 60 min per scanned and reassembled picture. Amongst AN samples a minimum of 2561 myelinated nerve fibres was measured, and at least 5280 fibres were included in work-up of common peroneal probes.

Morphometrical evaluation

The *endoneurial area* of individual AN fascicles ranged between 9443 and 148 798 μm^2 (Fig. 5). Thereby, different fascicles of one nerve revealed a scatter of about 45 000 μm^2. This finding is consistent with data obtained from the CPN (Table 1). Consequently, in terms of fascicular size variations, the two nerves did not differ significantly. Even within one fascicle a 1.5-cm distance bears a difference up to 4.026 μm^2.

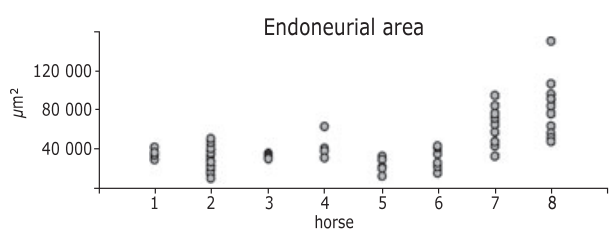

Fig. 5. Reference area variation amongst different AN fascicles and animals.

Similar features could be observed for *total myelinated fibre counts* in both accessory and CPN. Means and SD are displayed in Tables 1 and 2. The calculated *nerve fibre density* ranged between 3351/mm^2 and 17 812/mm^2 in AN samples and 5330/mm^2 and 12 956/mm^2 in the CPN samples. *Myelinated fibre diameter* distributions are exemplified in Fig. 6. The median, mean, peak, and percentage of myelinated fibres larger than 7-μm diameter [large myelinated fibres: (LMF)] are given in Table 2. Myelinated fibre sizes were between 2 μm (see settings) and 19-μm in ANs, but 16-μm in peroneal nerves. Thereby, histoplots exhibited a bimodal curve with an upper peak around 6 μm and a lower around 12.5 μm (Fig. 6). As histograms and the median fibre diameter indicate, most fibres belong to the small-diameter group. These fibres outnumber large ones by a factor of about 1.5 (Tables 1 and 2).

The degree of myelination was assessed in terms of *g-ratio* (Fig. 7). Across all animals, AN samples presented a *g-ratio* of 0.46–0.62. The mean *g-ratio* was calculated at 0.55 ± 0.001 (range: 0.46–0.63), which is close to those values obtained from CPN samples (0.47 ± 0.003; range: 0.42–0.56). Albeit being statistically insignificant, histoplots (Fig. 7) helped to uncover the tendency of an increase in *g-ratio* in the larger myelinated fibres. This trend could also be seen in histograms plotting the *myelin sheath diameter*. Here, in contrast to the fibre size, a 'large-fibre peak' is replaced by a slightly prolonged decay (Fig. 8). In about 60% of nerve fibres, myelin thickness measured between 1.8 and 2.4 μm in both accessory and CPN. The whole range encompassed a minimal value of 1.0 μm and a maximal value of 9.72 μm. Mean and median myelin-sheath diameters are 2.34 ± 0.53 and 2.22 in the accessory-, and 2.42 ± 0.52 and 2.29 in the CPNs.

Nerve fibre circularity was read from outer ($P2A^o$) and inner myelin margins ($P2A^i$) (Fig. 9). Thereby, whole fibre profiles revealed a mean form factor $P2A^o$ of 1.48 ± 0.45 in AN- and 1.42 ± 0.29 in peroneal nerve samples. Inner myelin margins appeared less circular in both the samples of nerves

Table 1. Comparative morphometry of accessory and common peroneal nerves (CPN)

Parameter	Accessory nerve	CPN
Fascicular area (μm^2)*	39 331.30 ± 22 035.11 33 349.97	32 441.82 ± 7590.92 31 261.58
Nerve fibre density (per mm^2)#	10 822.76 ± 635.03	9830.86 ± 667.82
Nerve fibre diameter (μm^2)*	7.18 ± 3.25 6.18	6.43 ± 2.09 5.96
% LMF	37.50	38.83
G-ratio#	0.55 ± 0.001	0.47 ± 0.003
Myelin sheath diameter (μm^2)*	2.34 ± 0.53 2.22	2.42 ± 0.52 2.29
Outer myelin sheath circularity*	1.48 ± 0.45 1.36	1.42 ± 0.29 1.34
Inner myelin sheath circularity*	2.43 ± 1.81 1.83	2.12 ± 1.19 1.69

LMF, large myelinated fibre.
*Data are expressed as mean ± SD, and median.
#Data are expressed as mean ± SD.

Table 2. Nerve fibre parameters in the healthy accessory nerve

Parameter	1	2	3	4	5	6	7	8
Fibre diameter* (μm)	7.00 ± 3.31 (5.82)	6.29 ± 2.30 (5.65)	6.63 ± 2.43 (5.97)	5.39 ± 1.85 (4.88)	5.18 ± 1.68 (4.75)	6.71 ± 2.43 (5.87)	8.07 ± 3.79 (6.82)	8.93 ± 3.93 (7.86)
First peak (μm)	< 6.0	< 5.5	< 6.5	< 5.0	< 4.5	< 6.5	< 7.0	< 8.0
Second peak (μm)	< 13.0	< 10.5	< 14.5	< 10.5	< 9.5	< 13.0	< 15.5	< 15.0
% LMFs	36.7	26.1	21.5	16.6	11.9	28.2	46.3	65.2
Myelin sheath diameter* (μm)	2.32 ± 0.54 (2.20)	2.29 ± 0.47 (2.19)	2.34 ± 0.42 (2.27)	2.17 ± 0.40 (2.10)	2.18 ± 0.36 (2.13)	2.19 ± 0.39 (2.15)	2.30 ± 0.49 (2.19)	2.71 ± 0.66 2.62
G-ratio#	0.53 ± 0.003	0.51 ± 0.004	0.50 ± 0.003	0.50 ± 0.005	0.46 ± 0.005	0.57 ± 0.002	0.62 ± 0.003	0.53 ± 0.003
Outer circularity*	1.46 ± 0.31 (1.38)	1.48 ± 0.34 (1.37)	1.47 ± 0.32 (1.40)	1.35 ± 0.28 (1.27)	1.47 ± 0.30 (1.37)	1.43 ± 0.24 (1.36)	1.47 ± 0.34 (1.37)	1.60 ± 0.83 1.36
Inner circularity*	2.28 ± 1.20 (1.90)	2.22 ± 1.22 (1.76)	2.68 ± 1.42 (2.27)	1.91 ± 1.34 (1.47)	2.12 ± 0.99 (1.78)	2.20 ± 1.25 (1.81)	2.37 ± 1.70 (1.69)	3.04 ± 3.03 1.85

LMF, large myelinated fibre.
*Data are expressed as mean ± SD, and median.
#Data are expressed as mean ± SD.

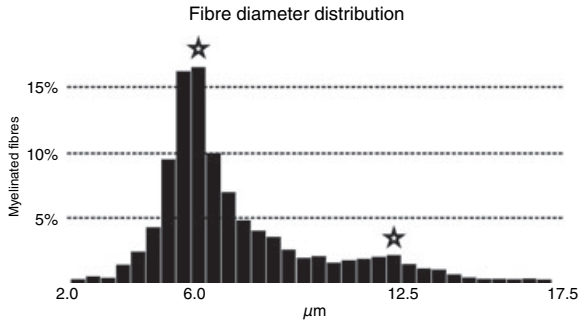

Fig. 6. This histogram highlights the bimodal fibre diameter distribution in the accessory nerve. Small Aβ/γ-fibres outnumber large myelinated motor axons and Ia/b-afferents, and peak around 6.0 μm diameter. Large myelinated fibres form another peak at 12.5 μm.

investigated, and presented a $P2A^i$ of 2.43 ± 1.81 and 2.12 ± 1.19, respectively. Also with these parameters statistically significant deviations are lacking amongst the two different biopsy sites.

Discussion

Accomplishing earlier reports on the diagnostic value of an AN biopsy in horses, our study proves for the first time its suitability for stereological assessment and the general representativity of its nerve fibre composition.

The subfascial topography, dorsomedial to sternocephalicus muscle at the lateral neck, guarantees (1) easy surgical exploration (Jackson et al., 1996) and (2) protection from incidental trauma, which otherwise would interfere with the suitability for assessment of intrinsic nerve diseases. This nerve branch is fixed in location and provides an adequate length for both semi-thin sectioning and nerve fibre teasing.

Once obtained, easy separation of single fascicles renders stretch- and crush artefacts minimal. Distortion of endoneurial structures never exceeded the threshold of 5% endoneurial area and 3% myelinated fibres, thereby, fulfilling reasonable sampling criteria (Sundkvist et al., 2000). In rare cases of enhanced fibroplasia, mesoneurial compaction can be overcome easily by repeated dipping into collagenolytic glycine buffer without remarkable chemical damage to myelin substance (Wieczorek, 2000).

Apart from its privileged topology and rather artefact-free obtainment, the histological appearance of the AN proved suitable for semi-automatic image analysis. Species-related frequency of subperineurial Renaut bodies (Jackson et al., 1996) was successfully counteracted by referring the endoneurial area to the area circumscribed by a line around outermost nerve fibres. Interactive steps, including fibre separation, joining-up of incomplete myelin sheaths, and deletion of PPD-positive debris, required 45–60 min per cross section at the most. This time frame is superior to the 3-h period considered necessary for morphometrical analysis of tibial and peroneal nerves in rats (Geuna et al., 1999).

In our setting, provision of whole trunk information was mandatory for evaluating the total composition of the AN under avoidance of size- and location-related bias (Geuna et al., 1999). For clinical evaluation, however, simple random sampling concerning about 185 out of 2900 fibres (Mayhew and Sharma, 1984) appeared appropriate for the equine LPN

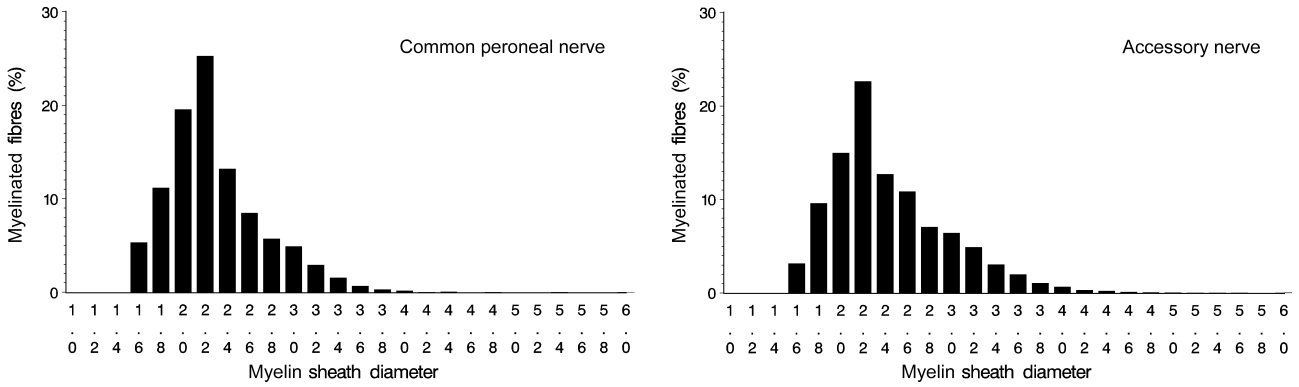

Fig. 7. Bar chart featuring the distribution of myelin sheath diameters within the fibre populations of the common peroneal and accessory nerve. Nerve fibres with myelin thickness of 2.2 μm are most frequent in both nerves.

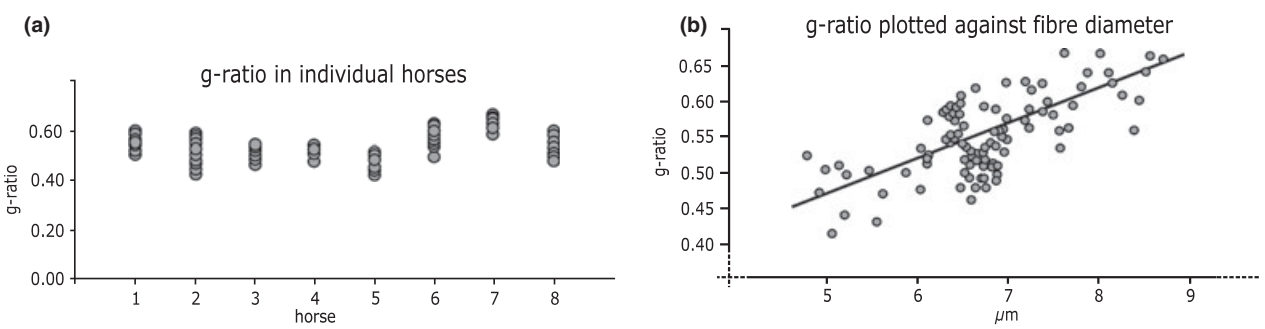

Fig. 8. The g-ratio of AN nerve fibres does not differ significantly between the animals investigated (a). Throughout all specimens, larger fibres tend to exhibit slightly higher g-ratios indicated by the calculated regression line (b).

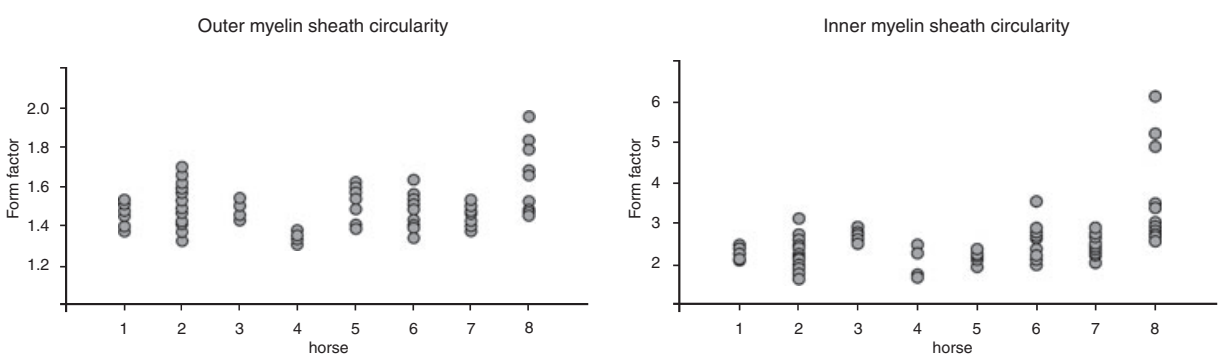

Fig. 9. In healthy AN, circularity of inner and outer myelin border behave similar; although the outer lining appears closer to a true circle. As discussed in the text, disorders of the peripheral nerve may result in asynchronous deviation from the reference range.

(Wheeler and Plummer, 1989) and it remains to be determined whether this kind of sampling is applicable to the AN as well. If so, a further decrease of turn-around time can be achieved.

The absolute number of myelinated nerve fibres usually is seen as predictor of impulse conductance while alterations in nerve fibre density reflect either fibre loss or, conversely, an increase on account of axonal sprouting at early stages of nerve regeneration. The present investigation revealed that in healthy subjects neither nerve fibre counts nor fibre density *per se* can be suggested as reliable parameters. Both values differ largely amongst all fascicles of the AN and the CPN, and they fail to exhibit significant differences between these two biopsy sites. With fibre counts ranging between 3351 and 17 812/mm^2 among AN samples and 5000 to 13 000/mm^2 in the CPN, their scatter of values is similar to that of the LPN that exhibits a mean around 6000 fibres per square millimetre (Wheeler, 1987). These findings support former notions (Dyck et al., 1984) that the fibre density in multi-fascicular nerves underlies significant inter- and intra-individual variations. Hence, in all three nerves, assessment of nerve fibre density is of limited value unless accomplished by fibre diameter histograms or two-dimensional distribution parameters.

Diameter histograms display the frequency distribution of distinct fibre calibres within a given fascicle. Not surprisingly, this study has shown that the equine AN presents with all myelinated fibre classes, including Aα-fibres (α-motor axons,

Ia/b-afferents) as well as mechanoceptor Aβ- and Aγ-afferents. Moreover, smaller mechano-, thermo- and nociceptive Aδ-afferents (< 2 μm) could be seen histologically albeit they were excluded from measurement through image segmentation (see settings). On its very origin, the accessory nerve contains motor fibres only. After leaving the caudal fossa via caudal foramen lacerum it gains post-ganglionic fibres from the cranial cervical ganglion, and sensory inputs from spinal nerves, mainly C2 and C3 (Nickel et al., 1984). That is how the extracranial AN portion gains somatomotor, somatosensory and parasympathetic fibre qualities.

Although most LMF in both AN and CPN ranged between 10 and 14 μm in diameter, a few measured up to 19 μm. These most probably resemble fast-conducting anulospiral Ia-afferents that have not yet been defined in equine peripheral nerves, while in cats they are known to differ from α-motor fibres by about 4 μm (Boyd and Kalu, 1979).

Like in most mammalian nerves of mixed fascicularity, the AN presents with a bimodal fibre diameter distribution, displaying an upper peak around 6 μm and a lower peak around 12.5 μm. In turn, this profile is similar to the equine common peroneal, deep peroneal (Slocombe et al., 1992), recurrent laryngeal (Slocombe et al., 1992) and sensory LPNs (Wheeler, 1987). If the recommended discrimination line between large and small myelinated fibres is drawn at 7–8 μm (Archibald et al., 1995; Wheeler and Plummer, 1989) slow Aβ- and Aγ-fibres (SMF) outnumber large Aα-fibres by a factor of about 1.5. Both peaks and this ratio have to be kept in mind approaching AN biopsies of possibly diseased animals as most degenerative, metabolic and toxic neuropathies affect distinct fibre classes to a different extent, leading to SMF:LMF-shifting and loss of bimodality (Dyck et al., 1984). Experienced raters may be able to estimate myelinated fibre densities with reasonable accuracy but proper assessment as to whether SMF or LMF are preferentially affected can only be reliably achieved by stereological methods (Pamphlett and Sjarif, 2003).

The calibre of a nerve fibre is positively correlated to its conduction velocity and inversely to both firing threshold and refractory period (Blair and Erlanger, 1933; Erlanger and Gasser, 1933). Thus, apart from providing qualitative information, diameter histograms enable the investigator to deduct electrophysiological properties that are blurred in clinical electroneurography (Vleggeert-Lankamp et al., 2004). The net conduction velocity of a myelinated nerve, on the other hand, can be estimated from the degree of myelination (Erlanger and Gasser, 1933). Physiologically, the myelin sheath thickness is related to both axonal diameter and inter-nodal length in a non-rectilinear manner (Wheeler, 1990). Unless accompanied by laborious teased fibre studies (Reynolds and Heath, 1995; Wheeler, 1990) peripheral nerve morphometry relies largely on two-dimensional analysis of cross sections. In humans, the axon-to-fibre relationship, referred to as *g-ratio*, should be close to 0.6 to guarantee optimal impulse transduction (Rushton, 1951). In the present study, most nerve fibres revealed a myelin thickness between 1.8 and 2.4 μm, and the overall *g-ratio* was calculated at 0.46 ± 0.005 to 0.62 ± 0.003. When plotted against fibre diameter, larger fibres showed an insignificant tendency to exhibit higher values. The *g-ratio* of ANs did not differ much from that of the CPN but ranged slightly below that found in the LPN (0.6 ± 0.065 to 0.73 ± 0.04) (Wheeler and Plummer, 1989). Conceivably, this difference is on account of lack of α-motor axons in the latter, and should be even more pronounced at early immature stages, when myelination in motor fibres precedes that of sensory nerves (Niebroj-Dobosz et al., 1980). Framed by the asynchronous development of axon and myelin sheath in neonates (Schroeder et al., 1988), and a larger scatter of values in aged individuals (Jacobs and Love, 1985) AN *g-ratios* of < 0.40 and > 0.65 are highly suggestive of encountering a hypermyelinated and hypomyelinated condition respectively.

A frequently employed parameter in stereological assessments that has to be treated with considerable caution is the myelin sheath circularity. As myelin sheath physiologically becomes constricted close to the node of Ranvier and impinged by perinuclear Schwann cell cytoplasm at mid-segmental areas, it has to be made sure that the measurement only includes stereotypic inter-nodal segments. In this setting, a large number of crenated profiles may indicate axonal atrophy with consecutive myelin sheath collapse. Given that a standardized fixation protocol is used, pathologically crenated fibres can be easily assessed by the form factor $P2A^o$ which orients along the outer margin of the myelin sheath. Myelinated AN fibres in our horses revealed a mean form factor of 1.48 ± 0.45 and, thereby, basically resemble peroneal nerve values (1.42 ± 0.3). Comparison to biopsy sites that are located more distally from the neuro-axis helps to uncover length-dependent axonal neuropathies of atrophy/dystrophy-type, such as sporadic and Australian stringhalt (Wheeler, 1987; Slocombe et al., 1992), at early stage. In single biopsy settings, implementation of age-related variations is mandatory as nerve fibre circularity is optimal when myelin sheath has been fully developed and thereafter gradually declines centripetally ascending, starting at the most distal aspects of the nerve (Schroeder et al., 1988). As another surrogate marker for axonal atrophy, the so-called inner myelin loops, protrudes into the peri-axonal space of Klebs, while the outer myelin surface retains its circularity. These fibres can be detected automatically if the form factor depends on the inner myelin border. With normal values of 2.43 ± 1.81 in ANs and 2.12 ± 1.19 in peroneal nerves the arising factor $P2A^i$ is remarkably higher and more scattered than $P2A^o$. Thus $P2A^i$ is less sensitive and algorithms including point count tools are superior to full automatic assessment. Nonetheless, obtainment of both form factors and the *g-ratio* are useful parameters to assess prolonged axonal degeneration *in statu nascendi*.

Taken together, comparative histology of the accessory- and CPNs demonstrated an equivalent nerve composition containing all myelinated fibre classes including Aα-, Aβ-, Aγ- and Aδ-types. Moreover, in healthy individuals most stereological parameters of AN, LPN and CPN present with the same range and scatter of values, in spite of varying distances to the CNS. Hence, distal neuropathies should lead to a considerable discrepancy between AN values and that obtained from farther sites, such as the LPN. Compared to the AN, however, LPN samples lack Aα-fibres larger than 15 μm and reveal a slightly lower *g-ratio*. Even in the absence of a second biopsy, the typical fibre diameter distribution and strictly regulated myelin sheath thickness serve as reliable quantitative parameters whenever visual assessment is lacking accuracy or electrophysiological properties require to be estimated.

Acknowledgements

The authors thank Claudia Maier, Sabine Sasz and Angela Siebert for excellent technical assistance. We are particularly grateful to Prof. Dr Hartmut Gerhards, Equine Clinic, LMU Munich, for making the nerve samples available.

References

Adams, C. W., Y. H. Abdulla, D. R. Turner, and O. B. Bayliss, 1968: Subcellular preparation of peripheral nerve myelin. Nature **220,** 171–173.

Archibald, S. J., J. Shefner, C. Krarup, and R. D. Madison, 1995: Monkey median nerve repaired by nerve graft or collagen nerve guide tube. J. Neurosci. **15,** 4109–4123.

Bailey, N. J. T., 1981: Statistical Methods in Biology, 2nd edn. London: Hodder & Stoughton.

Blair, E. A., and J. Erlanger, 1933: A comparison of the characteristics of axons through their individual electric responses. Am. J. Physiol. **106,** 524–564.

Boyd, I. A., and K. U. Kalu, 1979: Scaling factor relating conduction velocity and diameter for myelinated afferent fibers in the cat hind limb. J. Physiol. (Lond.) **289,** 287–297.

Cahill, J. I., B. E. Goulden, and R. D. Jolly, 1986: Stringhalt in horse: a distal axonopathy. Neuropathol. Appl. Neurobiol. **12,** 459–475.

Cochran, W. G., 1977: Sampling Techniques. New York: John Wiley & Sons.

Cummings, J. F., A. de Lahunta, C. George, L. Fuhrer, B. A. Valentine, B. J. Cooper, B. A. Summers, C. R. Huxtable, and H. O. Mohammed, 1990: Equine motor neuron disease: a preliminary report. Cornell Vet. **80,** 375–379.

Da Silva, A. P. D., C. E. R. Jordão, and V. P. S. Fazan, 2006: Peripheral nerve morphometry: comparison between manual and semi-automated methods in the analysis in a small nerve. J. Neurosci. Methods **159,** 153–157.

Duncan, I. D., 1992: Determination of the early age of onset of equine recurrent laryngeal neuropathy. Acta Neuropathol. (Berl.) **84,** 316–321.

Duncan, I. D., I. R. Griffiths, A. McQueen, and G. O. Baker, 1974: The pathology of equine laryngeal hemiplegia. Acta Neuropathol. (Berl.) **28,** 337–348.

Dyck, P. J., J. Karnes, P. O'Brien, N. Hitosh, A. Lais, and P. Low, 1984: Spatial pattern of nerve fiber abnormality indicative of pathologic mechanisms. Am. J. Pathol. **117,** 225–238.

Erlanger, J., and H. S. Gasser, 1933: Electrical Signs of Nervous Activity. Philadelphia: University of Philadelphia Press.

Fields, R. D., and M. H. Ellisman, 1986: Axons regenerated through silicone tube splices: II Functional morphology. Exp. Neurol. **92,** 61–74.

Geuna, S., P. Tos, B. Battiston, and R. Guglielmone, 1999: Verification of two-dimensional dissector, a method for the unbiased estimation of density and number of myelinated nerve fibers in peripheral nerves. Ann. Anat. **181,** 23–34.

Jackson, C. A., A. De Lahunta, J. F. Cummings, T. J. Divers, H. O. Mohammed, B. A. Valentine, and R. P. Hackett, 1996: Spinal accessory nerve biopsy as ante mortem diagnostic test for equine motor neuron disease. Equine Vet. J. **28,** 215–219.

Jacobs, J. M., and S. Love, 1985: Qualitative and quantitative morphology of human sural nerve at different ages. Brain **108,** 897–924.

Karnes, J., R. Robb, P. C. O'Brien, E. H. Lambert, and P. J. Dyck, 1977: Computerized image recognition for morphometry of nerve attribute of shape of sampled transverse sections of myelinated fibers which best estimates their average diameter. J. Neurol. Sci. **34,** 43–51.

Mayhew, T. M., and A. K. Sharma, 1984: Sampling schemes for measuring nerve fiber size. I. Method for nerve trunks of mixed fascicularity. J. Anat. **139,** 45–58.

Nickel, R., A. Schummer, and E. Seiferle, 1984: Lehrbuch der Anatomie der Haustiere IV. Nervensystem, endokrine Drüsen, Sinnesorgane, 2nd edn.Berlin: Paul Parey.

Niebroj-Dobosz, I., A. Fidzianska, J. Rafalowska, and E. Sawicka, 1980: Correlative biochemical and morphological studies of myelination in human ontogenesis: II Myelination of the nerve roots. Acta Neuropathol. (Berl.) **49,** 153–158.

Pamphlett, R., and A. Sjarif, 2003: Is quantitation necessary for assessment of sural nerve biopsies? Muscle Nerve **27,** 562–569.

Reynolds, R. J., and J. W. Heath, 1995: Patterns of morphological variation within internodes of normal peripheral nerve: quantitative analysis by confocal microscopy. J. Anat. **187,** 369–378.

Rodenacker, K., and E. Bengtsson, 2003: A feature set for cytometry on digitized microscopic images. Anal. Cell. Pathol. **25,** 1–36.

Romero, E., O. Cuisenaire, J. F. Denef, J. Delbeke, B. Macq, and C. Veraart, 2000: Automatic morphometry of nerve histological sections. J. Neurosci. Methods **97,** 111–122.

Rushton, W. A. H., 1951: A theory of the effects of fiber size in medullated nerve. J. Physiol. **115,** 101–122.

Schroeder, J. M., J. Bohl, and U. von Bardeleben, 1988: Changes of the ratio between myelin thickness and axon diameter in human developing sural, femoral, ulnar, facial, and trochlear nerves. Acta Neuropathol. (Berl.) **76,** 471–483.

Schultze, W. H., 1972: Über das Paraphenylendiamin in der histologischen Färbetechnik und über eine neue Schnellfärbemethode der Nervenmarkscheide am Gefrierschnitt. Zb. Pathol. **36,** 639–640.

Slocombe, R. F., P. J. Huntington, S. C. Friend, L. B. Jeffcott, A. R. Luff, and D. K. Finkelstein, 1992: Pathological aspects of Australian stringhalt. Equine Vet. J. **24,** 161–162.

Smith, K. J., 1978: A method to represent the spectrum of refractory periods of transmission of the constituent fibers of a nerve. J. Physiol. **288,** 7–9.

Sundkvist, G., L. B. Dahlin, H. Nilsson, K. F. Eriksson, F. Lindgard, I. Rosen, S. A. Lattimer, A. A. Sima, K. Sulliva, and A. D. Greene, 2000: Sorbitol and myo-inositol levels and morphology of sural nerve in relation to peripheral nerve function and clinical neuropathy in men with diabetic, impaired, and normal glucose tolerance. Diabetes Med. **17,** 259–268.

Tanck, J. J., 2004: Morphometric evaluation of peripheral nerve samples. Dr. med. vet. Thesis, Munich: Ludwig Maximilians University of Munich.

Urso-Baiarda, F., and A. O. Grobbelaar, 2006: Practical nerve morphometry. J. Neurosci. Methods **156,** 334–341.

Vleggeert-Lankamp, C. L. A. M., R. J. van den Berg, H. K. P. Feirabend, E. A. J. F. Lakke, M. J. A. Malessy, and R. T. W. M. Thomeer, 2004: Electrophysiology and morphometry of the Aα- and Aβ-fiber populations in the normal and regenerating rat sciatic nerve. Exp. Neurol. **187,** 337–349.

Wheeler, S. J., 1987: Structure and function of equine peripheral nerve: morphology, morphometry and clinical electrophysiology. PhD Thesis, London: University of London.

Wheeler, S. J., 1990: Quantitative and qualitative morphology of equine peripheral nerve: teased fiber studies. Res. Vet. Sci. **48,** 145–151.

Wheeler, S. J., and M. J. Plummer, 1989: Age-related changes in fiber composition of equine peripheral nerve. J. Neurol. Sci. **90,** 53–66.

Wieczorek, L., 2000: Nerve fiber teasing as a diagnostic aid in detection of peripheral neuropathies – methodology and interpretation. Dr. med. vet. Thesis, Munich: Ludwig Maximilians University of Munich.